Enhanced Diagnostic Capability for Glaucoma of 3-Dimensional Versus 2-Dimensional Neuroretinal Rim Parameters Using Spectral Domain Optical Coherence Tomography

Kenneth C. Fan, MD, MBA,† Edem Tsikata, PhD,†‡ Ziad Khoueir, MD,†‡§*
Huseyin Simavli, MD,†‡‖ Rong Guo, MS,†‡ Regina A. de Luna, BA,†¶
*Sumir Pandit, MD, MBA,‡ Christian J. Que, MD,†‡#**
Johannes F. de Boer, PhD,†‡††‡‡ and Teresa C. Chen, MD†‡

Downloaded from http://journals.lww.com/glaucomajournal by BhDMf5ePHKav1zEoum1tQfN4a+kJLhEZgbsIHo4XMi0hCywCX1AWnYQp/IlQrHD3i3D0OdRyi7TvSFl4Cf3VC1y0abggQZXdtwnfKZBYtws= on 02/09/2021

Purpose: To compare the diagnostic capability of 3-dimensional (3D) neuroretinal rim parameters with existing 2-dimensional (2D) neuroretinal and retinal nerve fiber layer (RNFL) thickness rim parameters using spectral domain optical coherence tomography (SD-OCT) volume scans.

Materials and Methods: Design: Institutional prospective pilot study. Study population: 65 subjects (35 open-angle glaucoma patients, 30 normal patients). Observation procedures: One eye of each subject was included. SD-OCT was used to obtain 2D RNFL thickness values and 5 neuroretinal rim parameters [ie, 3D minimum distance band (MDB) thickness, 3D Bruch's membrane opening-minimum rim width (BMO-MRW), 3D rim volume, 2D rim area, and 2D rim thickness]. Main outcome measures: Area under the receiver operating characteristic curve values, sensitivity, and specificity.

Results: Comparing all 3D with all 2D parameters, 3D rim parameters (MDB, BMO-MRW, rim volume) generally had higher area under the receiver operating characteristic curve values (range, 0.770 to 0.946) compared with 2D parameters (RNFL thickness, rim area, rim thickness; range, 0.678 to 0.911). For global region analyses, all 3D rim parameters (BMO-MRW, rim volume, MDB) were equal to or better than 2D parameters (RNFL thickness, rim area, rim thickness; *P*-values from 0.023 to 1.0). Among the three 3D rim parameters (MDB, BMO-MRW, and rim volume), there were no significant differences in diagnostic capability (false discovery rate >0.05 at 95% specificity).

Conclusions: 3D neuroretinal rim parameters (MDB, BMO-MRW, and rim volume) demonstrated better diagnostic capability for primary and secondary open-angle glaucomas compared with 2D neuroretinal parameters (rim area, rim thickness). Compared with 2D RNFL thickness, 3D neuroretinal rim parameters have the same or better diagnostic capability.

Key Words: primary open-angle glaucoma, spectral domain optical coherence tomography, 3-dimensional volume scan, minimum distance band, Bruch's membrane opening-minimum rim width

(*J Glaucoma* 2017;26:450–458)

Glaucoma is the leading cause of irreversible blindness in the world, currently affecting over 62.2 million people globally and over 3.3 million in North America.[1] Spectral domain optical coherence tomography (SD-OCT) has replaced time domain optical coherence tomography as the most widely used quantitative structural assessment of the optic nerve head (ONH) and the surrounding retinal nerve fiber layer (RNFL) for glaucoma.[2] These structural parameters remain essential in evaluating glaucoma since structural changes such as RNFL thinning often precede visual field deficits.[3,4] However, despite the advent of the newer 3-dimensional (3D) technical capabilities of SD-OCT, commensurate 3D software development has lagged behind; and current commercially available SD-OCT 3D software for glaucoma care needs further development.

Perhaps the most common SD-OCT imaging scan in glaucoma is the 2-dimensional (2D) peripapillary RNFL circle scan centered on the ONH. This methodology has some inherent diagnostic limitations due to ONH anatomic variability, myopia, glaucomatous RNFL reflectivity loss, peripapillary atrophy (PPA), and other issues.[5–15] For ONH evaluation, assessment has classically been quantified by the cup-to-disc ratio (CDR), and OCT can assess CDR by using a reference plane 150 μm above the retinal pigmented epithelium (RPE)/Bruch's membrane (BM) complex. However, these assessments are often unreliable due to variability of cup anatomy.[2,16] Furthermore, CDR assessment by OCT scanning reports can be ~0.1 higher

Received for publication June 11, 2016; accepted January 23, 2017.
From the *Boston University School of Medicine, Boston Medical Center; †Department of Ophthalmology, Massachusetts Eye and Ear Infirmary, Glaucoma Service; ‡Harvard Medical School, Boston, MA; §Beirut Eye and ENT Specialist Hospital, Beirut, Lebanon; ‖Department of Ophthalmology, Pamukkale University, Denizli, Turkey; ¶The Johns Hopkins University School of Medicine, Baltimore, MD; #University of the East Ramon Magsaysay Memorial Medical Center, Quezon City; **Romblon Provincial Hospital, Romblon, Philippines; ††Department of Physics and Astronomy, LaserLaB Amsterdam, VU University; and ‡‡Department of Ophthalmology, VU Medical Center, Amsterdam, The Netherlands.
T.C.C. has received funding from the National Institutes of Health UL1 RR 025758, Massachusetts Lions Eye Research Fund, Fidelity Charitable Fund (Harvard University), and the American Glaucoma Society Mid-Career Award (San Francisco, CA).
Disclosure: J.F.d.B.: Sponsored research Heidelberg Engineering, GmbH, Germany; Harvard Medical School-Center for Biomedical Optical Coherence Tomography Research and Translation Scientific Advisory Board Chair; Licenses to NIDEK Inc., Fremont, CA; Terumo Corporation, Tokyo, Japan; Ninepoint Medical, Cambridge, MA; and Heidelberg Engineering, GmbH, Germany. The remaining authors declare no conflict of interest.
Reprints: Teresa C. Chen, MD, Department of Ophthalmology, Harvard Medical School, Massachusetts Eye and Ear Infirmary, Glaucoma Service 243 Charles Street Boston, MA 02114 (e-mail: teresa_chen@meei.harvard.edu).
Copyright © 2017 Wolters Kluwer Health, Inc. All rights reserved.
DOI: 10.1097/IJG.0000000000000647

Copyright © 2017 Wolters Kluwer Health, Inc. All rights reserved.

than that determined clinically by glaucoma specialists.[17] In terms of future directions for OCT structural evaluation, studies have shown that 3D imaging parameters can demonstrate at least the same diagnostic capabilities as 2D RNFL thickness, can improve diagnostic sensitivity of glaucoma at 95% specificity, can track glaucomatous changes of acute intraocular pressure (IOP) elevation in nonhuman primate models, and can longitudinally evaluate structural changes secondary to glaucoma.[18–23] Therefore, there is clearly a need to develop and test 3D SD-OCT methods for interpreting glaucomatous neuroretinal rim changes,[24] because 3D algorithms may hold better potential than 2D methods for detecting subtle structural changes in the clinic.

Given the diagnostic potential of 3D imaging from past studies,[18–20,22–27] this study investigated 5 neuroretinal rim parameters to determine the best method of analyzing 3D volume data. This study specifically features two newer 3D neuroretinal rim parameters: the Bruch's Membrane Opening-Minimum Rim Width (BMO-MRW) and the "minimum distance band" (MDB) thickness. Using an SD-OCT radial scan protocol, past studies have defined the BMO-MRW as the neuroretinal rim bound by the shortest distance from BMO to the cup surface[19,20] and have demonstrated a stronger structure-function relationship in glaucomatous eyes with the BMO-MRW compared with RNFL thickness and other 2D parameters.[28] Using an SD-OCT raster volume scan protocol, our group has previously reported the MDB neuroretinal thickness parameter, which is a circular band that is bound by the shortest distance between the termination of the RPE/BM complex and the closest corresponding points along the cup surface.[2,29] Under this same SD-OCT raster volume scan protocol, we were also able to examine older 150 μm reference plane based neuroretinal rim tissue parameters including rim area, rim volume, and rim thickness. We hypothesize that newer 3D neuroretinal rim parameters (eg, MDB and BMO-MRW) are better at diagnosing glaucoma than the classic 2D parameters used today and that different SD-OCT scanning methods can offer new and additional parameters for ONH evaluation. Therefore, in this study, we evaluated the diagnostic capabilities of 3D and 2D neuroretinal parameters as well as 2D RNFL thickness from SD-OCT imaging in a group of primary and secondary open-angle glaucoma and normal patients who were imaged with the Spectralis instrument (Heidelberg Engineering, Heidelberg, Germany).

MATERIALS AND METHODS

Participants and Examinations

All study subjects were recruited from the Glaucoma Service at the Massachusetts Eye and Ear Infirmary between September 2014 and June 2015 as part of a study approved by the Massachusetts Eye and Ear Infirmary Institutional Review Board. All included patients provided informed consent in accordance with the Declaration of Helsinki for research involving human subjects as well as the Health Insurance Portability and Accountability Act Regulations. A glaucoma specialist (T.C.C.) examined all patients. Each patient's clinic visit documentation included history of present illness, best-corrected visual acuity, refraction, slit-lamp examination, Goldmann applanation tonometry, gonioscopy, and dilated ophthalmoscopy. All imaging and diagnostic procedures were performed for all patients on the same day and included Spectralis OCT imaging, stereo disc photography (Visucam Pro NM; Carl Zeiss Meditec Inc.), and Humphrey visual field (HVF) testing (Swedish Interactive Threshold Algorithm 24-2 test of the Humphrey visual field analyzer 750i; Carl Zeiss Meditec Inc.). Only 1 eye per patient was included in the study.

All patients were dilated for imaging (HRA/Spectralis software version 5.4.8.0). We performed 3 imaging protocols on each subject on the same day including: (1) circle scan for RNFL thickness; (2) 20×20-degree raster volume scan of the ONH for MDB thickness, rim volume, rim area, and rim thickness measurements; (3) radial scan of the ONH for BMO-MRW measurements, with manual correction of the BMO border in the clinic. Scans were only included if images: (1) had a signal strength ≥ 15 (range, 0 to 40)[30]; (2) had clear visibility of the fundus, optic disc, and RNFL; and (3) were continuous without significant blank areas. The automatic real-time eye-tracking system of the Spectralis OCT allowed for averaging of multiple scans at the same location.

From the 3 imaging protocols, we were able to investigate 6 diagnostic parameters: 2D RNFL thickness, 2D neuroretinal rim area, 2D neuroretinal rim thickness, 3D neuroretinal rim volume, 3D MDB thickness, and 3D BMO-MRW. RNFL thickness was determined by Heidelberg software and was obtained from Heidelberg Spectralis Exam Reports. The neuroretinal rim parameters (ie, rim volume, rim area, and rim thickness) and MDB thickness were calculated from the 3D ONH raster volume scans with software developed at the Massachusetts Eye and Ear Infirmary (Figs. 1, 2). This scan protocol consisted of 193 raster images over a region $\sim 6\,\text{mm} \times 6\,\text{mm}$. The RPE/BM complex (Fig. 1A, pink dotted circle) and the cup surface (Fig. 1B, yellow dotted circle) were reconstructed by segmenting the images. In accordance with previous definitions of the RPE/BM complex, we segmented the RPE/BM complex when we were able to identify either just the RPE, or just the BM, or both the RPE and BM.[31] For rim volume, rim area, and rim thickness, the traditional reference surface of 150 μm above the RPE/BM complex was used to calculate the ONH parameters (Fig. 1C with 150 μm reference plane represented by yellow letter Z).[16,32] Rim volume was calculated by measuring the tissue bounded below by the 150 μm reference surface, above by the internal limiting membrane, and radially by the RPE/BM complex). The rim area (Fig. 2A) was the projection of the rim volume (Fig. 2B, C) on a transverse plane. The rim thickness was the rim volume divided by the rim area. The MDB thickness was calculated by measuring the shortest distances from 100 points along the RPE/BM complex to the cup surface (Fig. 1D) and has been previously described in detail by our group in recent publications.[33,34] The BMO-MRW thickness was determined from the 24 radial B-scan protocol, using the Glaucoma Premium Module software (6.0.11) seen in Figure 3. The BMO-MRW is defined by the minimum distance between the BM opening and the internal limiting membrane.[19,35] The Glaucoma Premium Module software is commercially available and is FDA approved. For each of the 6 parameters, we measured a total of 9 regions: global, 4 quadrants (inferior, superior, nasal, and temporal), and four 45-degree sectors (inferonasal, superonasal, inferotemporal, and superotemporal).

Copyright © 2017 Wolters Kluwer Health, Inc. All rights reserved.

Copyright © 2017 Wolters Kluwer Health, Inc. All rights reserved.

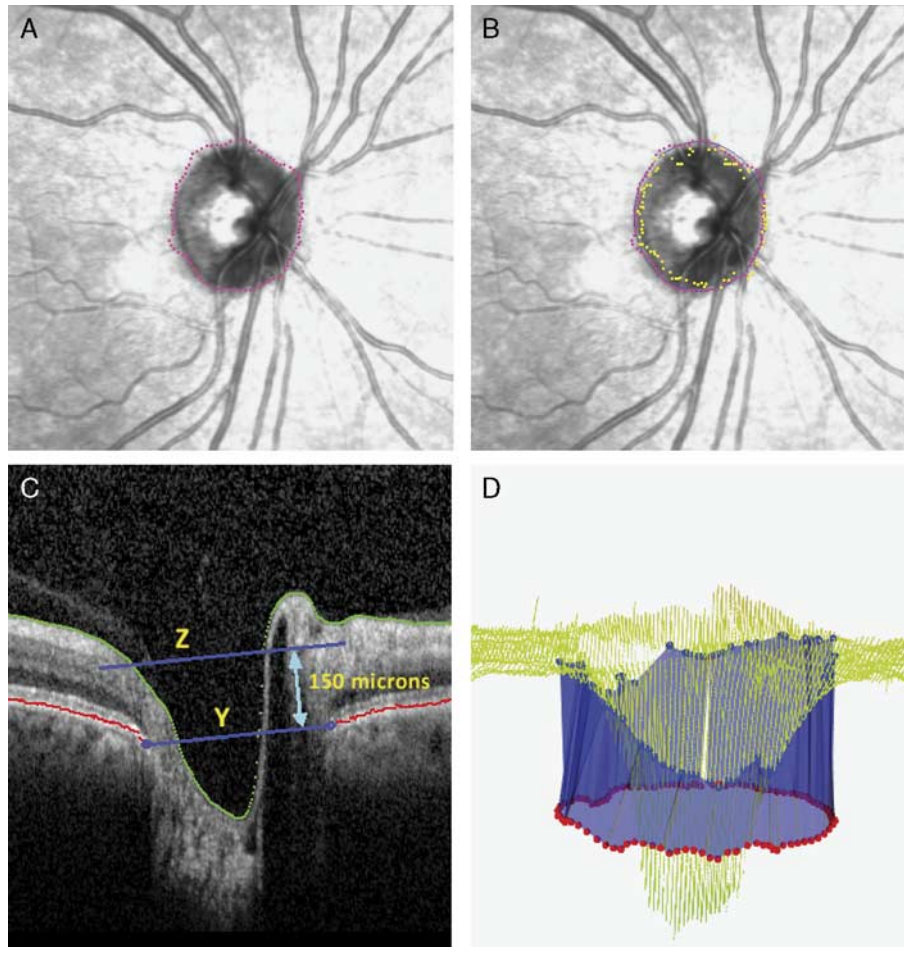

FIGURE 1. Depiction of how neuroretinal rim parameters were derived from the raster volume scan protocol. This example is of a normal right eye. After volume scans were obtained with Spectralis optic coherence tomography (OCT) imaging (HRA/Spectralis software version 1.9.1.0, Heidelberg Engineering, Heidelberg, Germany), custom-designed Massachusetts Eye and Ear Infirmary software calculated (A and C) rim area, rim volume, and rim thickness and (B and D) minimum distance band (MDB) thickness. A, The pink dotted circle represents the OCT-based disc border, or retinal pigmented epithelium (RPE)/Bruch's membrane (BM) complex termination. B, The yellow dotted circle represents the cup surface points which are closest to the OCT-based RPE/BM complex border, which defines the outer MDB border (D, pink dotted circle). C, B-scan, where yellow letter Y represents the RPE/BM complex plane, and yellow letter Z represents the 150 μm reference plane which is 150 μm above the RPE/BM complex and which divides the neuroretinal rim above from the cup below. D, MDB as a 360-degree circumferential blue band, which is bordered above by the cup surface (blue dotted circle) and below by the OCT-based RPE/BM complex (pink dotted circle).

The inclusion criteria for this study were as follows: (1) patients who received a dilated eye exam, disc photos, HVF testing, Spectralis RNFL scan, SD-OCT 3D ONH raster volume scan, and Spectralis BMO-MRW scans on the same day; (2) spherical equivalent between −5.0 D to +5.0 D inclusive; and (3) reliable HVF test results with ≤33% fixation losses, ≤20% false-positive results, and ≤20% false-negative results. Patients were excluded from the study if there was presence of congenital anomalies of the anterior chamber, corneal scarring or opacities, HVF loss attributable to a nonglaucoma condition, such as central retinal vein or artery occlusion or panretinal photocoagulation, dilated pupillary diameter <2 mm, or severe nonproliferative or proliferative diabetic retinopathy. Only patients with best-corrected visual acuity of 20/50 or better were included in this study.

In selecting glaucoma subjects for this study, we included primary and secondary forms of open-angle glaucoma. The following types of open-angle glaucoma were included: primary open-angle glaucoma, normal tension glaucoma, pseudoexfoliation glaucoma, and pigmentary glaucoma. Any patient diagnosed with chronic angle closure glaucoma, traumatic glaucoma, aphakic glaucoma, juvenile open-angle glaucoma, or uveitic glaucoma was excluded from the study. All diagnoses were confirmed by a glaucoma specialist (T.C.C.). To qualify for a diagnosis of glaucoma, an abnormal VF was defined by either 3 or more contiguous pattern SD (PSD) test locations depressed by 5 dB or more; or 2 or more contiguous PSD test locations with 1 depressed by 10 dB or more and the other by 5 dB or more. Abnormal PSD test locations on the outer rim of the visual field were not considered in the aforementioned criteria to account for peripheral rim artifacts.

For normal subjects, patients were included if they satisfied the following criteria: (1) absence of other ocular

Copyright © 2017 Wolters Kluwer Health, Inc. All rights reserved.
Copyright © 2017 Wolters Kluwer Health, Inc. All rights reserved.

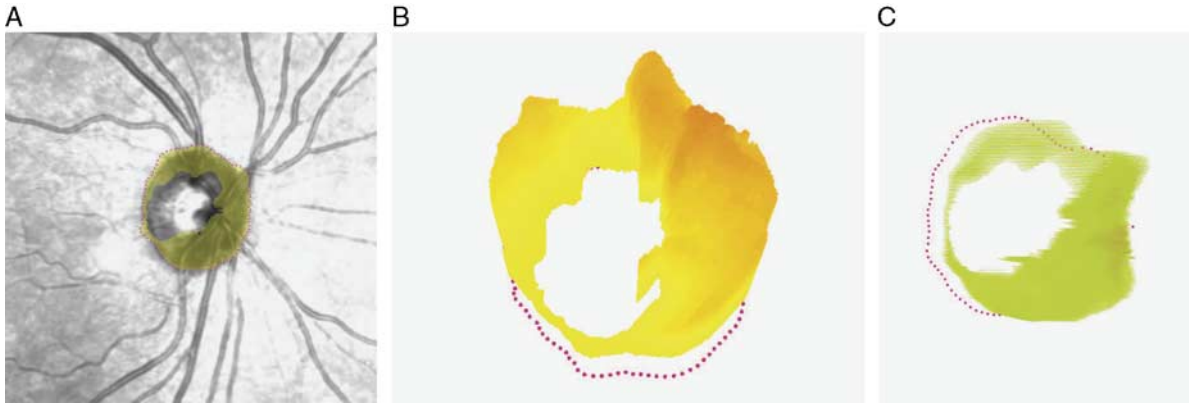

FIGURE 2. Depiction of neuroretinal rim parameters derived from the raster volume scan protocol (ie., neuroretinal rim volume, rim thickness, and rim area). This example is the normal right eye who had volume scans using Spectralis optical coherence tomography (OCT) imaging (HRA/Spectralis software version 1.9.1.0, Heidelberg Engineering, Heidelberg, Germany). Using our custom-designed algorithm, the OCT-based retinal pigmented epithelium (RPE)/Bruch's membrane (BM) complex border is shown as pink dotted circles in (A–C) and represents the termination of the RPE/BM complex. A, The integrated reflectance image shows the rim area in yellow. B and C, Three-dimensional representations of rim volume, which is 150 μm above the OCT-based RPE/BM complex border (pink dotted circles).

disease with the exception of mild cataracts; (2) normal HVF test results as defined by hemifield test results within normal limits; and (3) CDR asymmetry ≤ 0.2 between eyes. No patients with physiologic cupping were included, and CDRs for whites were ≤ 0.4 and for African Americans and Hispanics ≤ 0.6.

For patients where both eyes were eligible for inclusion, 1 eye was selected at random using the Microsoft Excel 2010 (Microsoft Corporation, Redmond, WA) random number generator function " = RANDBETWEEN(min,max)." Defining "min" as "1," and "max" as "2," we assigned the value "1" to indicate selection of the left eye and "2" to indicate selection of the right eye.

Statistical Analysis

Results are reported as means ± SD, unless otherwise stated. χ^2 or 2 sample t tests were used for the comparison of demographic variables between normal and glaucoma patients.

For all 9 regions of our 6 parameters (RNFL thickness, MDB thickness, rim area, rim volume, rim thickness, BMO-MRW), we determined area under the receiver operating characteristic (AUROC) curve values. To find the most accurate diagnostic parameter for glaucoma, AUROC curve values were evaluated with pairwise comparisons, and false discovery rates were calculated to adjust for the multiple comparisons. P-values < 0.05 were considered statistically significant. All statistical analyses were performed using SAS 9.4 (SAS Institute Inc., Cary, NC).

RESULTS

There were 65 patients in our study, 35 glaucoma subjects and 30 normal subjects, with mean age of 67.7 ± 11.0 and 58.5 ± 12.0 years, respectively (P-value < 0.01, Table 1). Statistically significant differences were also found in clinically assessed CDR as well as HVF mean and pattern SD (Table 1). Of the glaucoma subjects, 51.4% (18/35) were categorized as early glaucoma (HVF mean deviation > -6 dB, inclusive) and 48.6% (17/35) as moderate to severe glaucoma (HVF mean deviation worse than -6 dB).

Table 2 shows the AUROC values for all 9 regions for the 6 parameters investigated in our cohort. Four of the 5

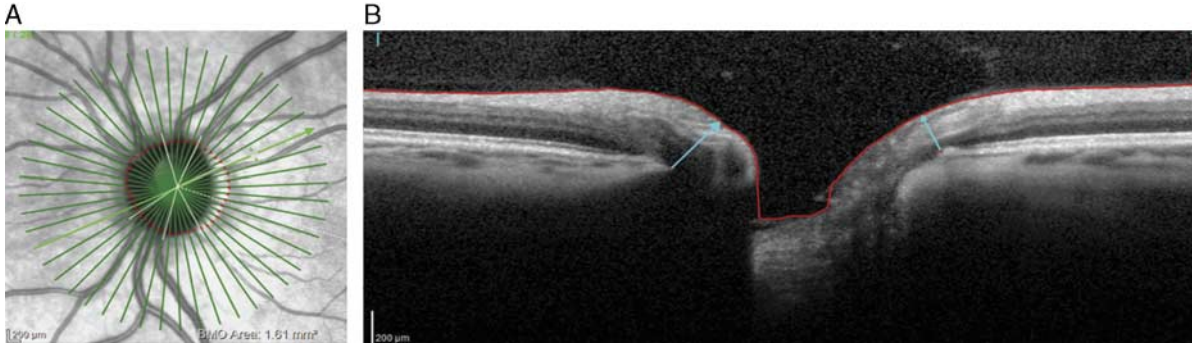

FIGURE 3. Representative integrated reflectance image (A) and associated B-scan (B) of the Bruch's membrane opening-minimum rim width (BMO-MRW) scan protocol from Heidelberg Spectralis OCT (HRA/Spectralis software version 1.9.1.0, Heidelberg Engineering GmbH, Heidelberg, Germany). A, The 24 radial B-scan protocol for measuring the BMO-MRW is shown. The highlighted green line represents the radial B-scan shown on the right in picture B, BMO-MRW is a measurement of the minimum distance (light blue arrows) between the internal limiting membrane and BMO.

Copyright © 2017 Wolters Kluwer Health, Inc. All rights reserved.

Copyright © 2017 Wolters Kluwer Health, Inc. All rights reserved.

TABLE 1. Demographics of the Primary Open-Angle Glaucoma and Normal Study Populations

	POAG	Normal	*P*
No. eyes	35	30	
No. right eyes/left eyes	20/15	11/19	
Sex (male/female)	18/17	13/17	0.515
Age (y)	67.7 ± 11.0	58.5 ± 12.0	0.002
Refractive error (spherical equivalent D)	−0.20 ± 1.62	−0.76 ± 1.88	0.202
Cup-to-disc ratio*	0.67 ± 0.17	0.4 ± 0.18	< 0.0001
Visual field†			
Mean deviation (dB)	−8.15 ± 7.35	−1.78 ± 1.88	< 0.0001
Pattern SD (dB)	6.29 ± 3.82	1.78 ± 0.79	< 0.0001
Race	35	30	0.811
White	4	3	
African American	22	22	
Asian	7	4	
Hispanic	1	0	
Other‡	1	1	

All results are described in the format of mean ± SD unless indicated otherwise.

*Cup-to-disc ratio as performed through clinical assessment by trained ophthalmologist.

†Visual field data obtained through Humphrey's Visual Field testing.

‡"Other" racial group represents a patient of unspecified European descent.

POAG, primary open-angle glaucoma.

top AUROC curve values were for 3D parameters: BMO-MRW inferotemporal [0.946; 95% confidence interval (CI), 0.89-0.99], BMO-MRW global [0.928 (95% CI, 0.86-0.99)], BMO-MRW inferior [0.927 (0.86-0.99)], rim volume inferotemporal (0.917 [0.85-0.99]), and rim thickness inferotemporal (0.911 [0.84-0.99]). As seen in Table 2, global values of 3D rim parameters (BMO-MRW, rim volume, and MDB thickness) were equal to or better than 2D parameters (RNFL thickness, rim area, rim thickness; *P*-values ranging from 0.023 to 1.0). In comparisons for diagnostic ability of the 3D rim parameters as determined by AUROC values using false discovery rates, no statistically significant differences were detected. When pairwise comparisons were done between 3D and 2D parameters for global and quadrant regions, we found that 3D parameters were similar to 2D parameters, except for the following pairs: 3D BMO-MRW better than 2D RNFL (nasal $P = 0.035$, temporal $P = 0.037$), 3D BMO-MRW better than 2D rim area (global $P = 0.023$, inferior $P = 0.009$, and temporal $P = 0.036$), 3D BMO-MRW better than 2D rim thickness (superior $P = 0.014$, nasal $P = 0.031$, and temporal $P = 0.036$), and 3D rim volume better than 2D rim area (inferior $P = 0.018$).

Figures 4 and 5 depict the AUROC graphs for visual comparison between RNFL, BMO-MRW, MDB, and RNFL thickness, demonstrating that at ~95% specificity, BMO-MRW, MDB thickness, rim volume, and RNFL thickness yielded sensitivity values of 86%, 83%, 68%, and 60%, respectively. Fig. 5 shows the AUROC curves for MDB thickness, BMO-MRW, rim volume, and RNFL for the 4 quadrants and 4 sectors. In Fig. 5, there is a trend for RNFL thickness having lower total AUROC curves as compared with all three 3D neuroretinal rim parameters (ie, MDB thickness, BMO-MRW, and rim volume).

DISCUSSION

Our study demonstrates that 3D neuroretinal rim parameters obtained by SD-OCT imaging may be superior to 2D SD-OCT diagnostic tools in differentiating glaucoma from normal patients. Similar to patterns established in previous studies,[36,37] we also found that the inferior quadrant and inferotemporal sector more consistently exhibited higher diagnostic capabilities compared with other regions for all 6 measured parameters (Table 2).[9,22,38–41] Using AUROC curves as an indicator for diagnostic capability, our results illustrate that the diagnostic performance of these 3D neuroretinal rim parameters (ie, MDB thickness, BMO-MRW, and rim volume) exceeds that of 2D RNFL thickness in almost all quadrants and sectors (Table 2). Also, Figures 4 and 5 illustrate a trend that sensitivity and AUROC curve values for these 3D neuroretinal rim parameters were superior to the 2D RNFL parameter. On the basis of our results, the development of new 3D SD-OCT parameters may augment or supplement the diagnostic capability of existing SD-OCT parameters, such as 2D RNFL thickness.

Multiple groups have acknowledged the advantages of 3D OCT imaging as well as the disadvantages of 2D RNFL thickness measurements in glaucoma. For example, groups

TABLE 2. Comparison of Diagnostic Capability of Retinal Nerve Fiber Layer and 5 Neuroretinal Rim Ocular Coherence Tomography Parameters for Primary Open-Angle Glaucoma

	2D RNFL Thickness	3D MDB Thickness	3D BMO-MRW	3D Rim Volume	2D Rim Area	2D Rim Thickness
	AUROC (SE)	AUROC (SE)	AUROC (SE)	AUROC (SE)	AUROC (SE)	AUROC (SE)
Global	0.850 (0.046)	0.884 (0.045)	0.928 (0.036)	0.892 (0.042)	0.837 (0.050)	0.884 (0.043)
Inferior	0.875 (0.043)	0.903 (0.042)	0.927 (0.036)	0.905 (0.040)	0.821 (0.051)	0.910 (0.039)
Superior	0.816 (0.052)	0.811 (0.056)	0.875 (0.042)	0.842 (0.050)	0.792 (0.058)	0.793 (0.056)
Nasal	0.721 (0.065)	0.831 (0.053)	0.867 (0.045)	0.835 (0.050)	0.815 (0.054)	0.795 (0.055)
Temporal	0.678 (0.067)	0.796 (0.054)	0.838 (0.049)	0.770 (0.058)	0.735 (0.061)	0.725 (0.063)
Superotemporal	0.818 (0.053)	0.790 (0.057)	0.877 (0.042)	0.830 (0.050)	0.783 (0.059)	0.799 (0.054)
Inferotemporal	0.869 (0.046)	0.885 (0.043)	0.946 (0.026)	0.917 (0.036)	0.818 (0.053)	0.911 (0.038)
Superonasal	0.760 (0.059)	0.823 (0.056)	0.870 (0.043)	0.819 (0.056)	0.783 (0.060)	0.776 (0.060)
Inferonasal	0.806 (0.055)	0.889 (0.044)	0.902 (0.041)	0.871 (0.046)	0.803 (0.053)	0.861 (0.047)

All results are described in the format of mean (SE) unless indicated otherwise.

AUROC indicates area under the receiver operating characteristic; 2D indicates 2-dimensional; 3D, 3-dimensional; BMO-MRW, Bruch's membrane opening -minimum rim width; MDB, minimum distance band; POAG, primary open-angle glaucoma; RNFL, retinal nerve fiber layer.

Copyright © 2017 Wolters Kluwer Health, Inc. All rights reserved.

Copyright © 2017 Wolters Kluwer Health, Inc. All rights reserved.

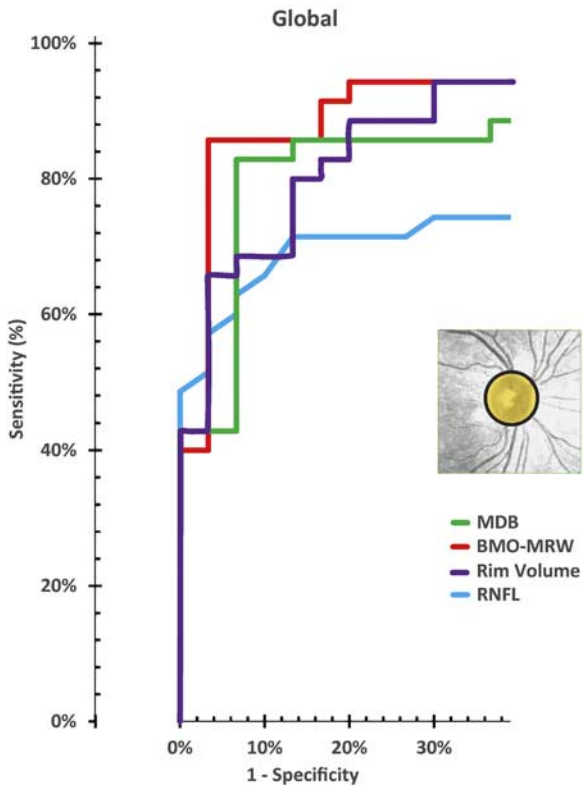

FIGURE 4. The diagnostic capabilities and area under the receiver operating characteristic curves for gold standard 2-dimensional (2D) retinal nerve fiber layer (RNFL) versus 3-dimensional (3D) global neuroretinal rim parameters [Bruch's membrane opening-minimum rim width (BMO-MRW), minimum distance band (MDB), rim volume].

have suggested that the 3D BMO-MRW not only may have better diagnostic capability compared with 2D RNFL thickness in humans (AUROC, 0.96 vs. 0.92, respectively),[19] but may also have better structure-function correlation with visual field defects ($P < 0.01$).[25,28] Our group has also shown that peripapillary retinal thickness parameters derived from 3D volume scans have excellent diagnostic capability with fewer algorithmic errors for detecting glaucoma as compared with peripapillary RNFL thickness ($P = 0.03$).[22] According to this[22] and other papers, the performance of many 3D imaging parameters are not as affected by RNFL reflectivity loss, myopia, and PPA in preliminary investigations.[9,42] Unlike some 3D parameters, the reliability of RNFL thickness as a diagnostic indicator decreases in such scenarios, for example when there is PPA or RNFL reflectivity loss due to advanced glaucoma, or when measurements are made in nasal quadrants.[6,8,9] In addition, RNFL thickness is measured around a 3.4 mm or more diameter circle centered on the ONH.[5,7,9,21] However, the lack of a true anatomic landmark as the focal center for circle scans allows for inaccuracies in RNFL measurements due to decentration,[19,21] which has been reported in even 27.8% of RNFL scans.[43] It has been reported that for mild to advanced glaucoma, 70% to 94% of RNFL defects are diffuse in nature with some patients exhibiting changes only nearer to the RPE/BM complex.[18] As such, measuring at a fixed distance from the disc can lead to misdiagnosis in certain patients, because there are individual as well as ethnic variations in disc size and because the RNFL is normally thicker closer to the RPE/BM complex. Unlike 2D RNFL circle scans, 3D parameters (ie, MDB thickness and rim volume) described in this study are derived from 20×20-degree ONH volume raster scans that are capable of gathering data from the entire retina surrounding the ONH. These volume scans do not face the same limitations as RNFL thickness and can be considered as the next step for diagnostic imaging in glaucoma, because 3D volume scans are not as affected by an artifact in a single frame compared with a 2D scan which consists of just a single frame or B-scan. Plus, the peripapillary 2D RNFL thickness circle scan and the BMO-MRW radial scan are both largely focused on imaging a singular anatomic tissue, that is, the RNFL and the neuroretinal rim, respectively. In contrast, a single 3D ONH volume scan can generate many parameters, such as cup volume, MDB thickness and area, rim volume, rim area, rim thickness, peripapillary retinal thickness[22] and volume, and peripapillary RNFL thickness and volume. Therefore, the results of this study are in agreement with past evidence that suggest that 3D SD-OCT derived parameters and 3D volume scans are superior to 2D parameters and are not subject to the same limitations of RNFL thickness measurements.

In comparing 3D neuroretinal rim parameters derived from volume raster scans (MDB thickness, rim volume) with those derived from radial scans (BMO-MRW), our study did not show any significant differences in diagnostic capability among 3D raster scan parameters and 3D radial scan parameters (ie, false discovery rate P-values > 0.05). Although there are no large studies which specifically compare BMO-MRW radial versus MDB raster scan protocols for rim parameters, the inherent differences in actual area scanned may temper the study design and conclusions of any such a study. The BMO-MRW radial scan is performed through radial cuts that are corrected according to the Fovea-BMO center (FoBMO) axis. The diagnostic utility of this feature has yet to be established and are currently inconclusive. A recent study by Mwanza et al[44] has shown that adjustments made according to the fovea-disc angle have no consistent effect on diagnostic performance.[26,45] However, it has been demonstrated by He et al[46] that the rotation of the radial scans along the FoBMO axis results in a significantly shifted alignment between BMO-MRW scans and those not utilizing the FoBMO axis correction, thereby resulting in pairwise comparisons between non-identical quadrants and sectors. Future larger studies are needed to better define the differences between the MDB thickness parameter with associated 3D raster volume scan and the BMO-MRW parameter with associated radial scan protocol.

In terms of the image acquisition time and the resulting number of parameters procured, the 3D raster volume scan may have several advantages over the BMO-MRW radial scan protocol. For example, there are extra manual steps involved in the BMO-MRW radial scan protocol that may have contributed to its slightly improved, although not statistically better, diagnostic capability compared with raster scan parameters (ie, MDB thickness and rim volume; Table 2). Before the BMO-MRW radial scan is done, one ideally needs to obtain corneal curvature readings from a keratometer and then input that corneal data

Copyright © 2017 Wolters Kluwer Health, Inc. All rights reserved.

Copyright © 2017 Wolters Kluwer Health, Inc. All rights reserved.

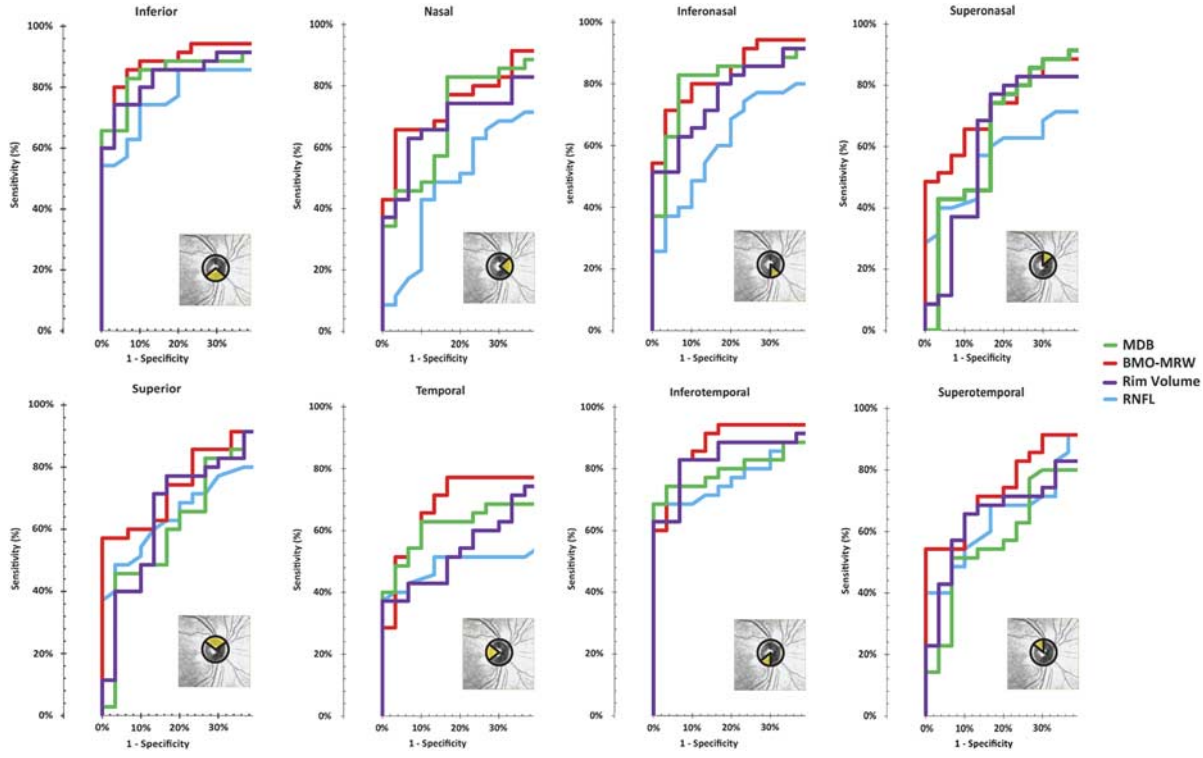

FIGURE 5. The diagnostic ability and area under the receiver operating characteristic curves for gold standard 2-dimensional (2D) retinal nerve fiber layer thickness (RNFL) versus 3-dimensional (3D) neuroretinal rim parameters [Bruch's membrane opening-minimum rim width (BMO-MRW), minimum distance band (MDB), rim volume]. The 8 regions depicted include 4 quadrants (ie, inferior, superior, nasal, and temporal) and 4 sectors (ie, superotemporal, inferotemporal, superonasal, and inferonasal).

into the Heidelberg Spectralis imaging device. Then the operator must determine the FoBMO axis. Then for this study, manual correction of the BMO border during the scan process was performed in the clinic for the 24 radial BMO-MRW scans. In contrast, for the MDB raster scan protocol, no individualized keratometry readings or manual correction of the RPE/BM complex was done during the scan process. Therefore, for this study, the BMO-MRW measurements with keratometry readings and with BMO manual corrections took up to 10 minutes per subject and resulted in neuroretinal rim measurements, whereas the 3D volume raster scan took <2 minutes and resulted in cup, neuroretinal rim, RNFL, and peripapillary retinal parameters (ie, cup volume, MDB thickness and area, rim volume, rim area, rim thickness, peripapillary retinal thickness[22] and volume, and peripapillary RNFL thickness and volume). It should be noted that for the MDB and other raster scan-derived parameters, poor-quality frames in the dataset were manually identified and automatically corrected by interpolation from good data using the in-house algorithm. Given the differing methods of image quality control, further studies are needed comparing the diagnostic ability of the BMO-MRW to the MDB thickness parameter, where correction of segmentation data for both radial and raster scan protocols is standardized and also comparable between studies. For example, in contrast to a study by Pollet-Villard et al,[28] the MDB thickness in our study was calculated without manual measurement of the neuroretinal rim tissue thickness. The raster line scan protocol presented also offers the advantage of having a higher density of information in the periphery near the RPE/BM complex and in the peripapillary region, as opposed to the radial scan protocol which has the lowest density of information in the peripapillary region and the highest density of information in the cup center, where there is usually space and no clinically useful data. As such, although 3D rim parameters have similar diagnostic capability for glaucoma, the 3D raster volume scan in particular may be an important tool to augment the current standard of care in glaucoma OCT imaging.

There were some limitations to our study. Our RNFL AUROC curve values were lower than other comparison studies (Table 2),[9,36] and this may have been because our population contained a higher percentage of early glaucoma subjects (51%) compared with other studies. In addition, another study needs to be done to see if acquiring the BMO-MRW without manual correction of the BMO border in the clinic and without keratometry readings yields similar diagnostic capability as the MDB scan protocol which does not need either manual adjustment of the RPE/BM complex in the clinic and which does not need keratometry readings. The small sample size of our study also necessitates larger studies evaluating these new 3D glaucoma OCT parameters, but the current study does generate new hypotheses for these future studies.

In conclusion, this study corroborates existing literature that 3D neuroretinal rim parameters which utilize anatomic landmarks derived from SD-OCT imaging are useful in enhancing the current standard of care in glaucoma

Copyright © 2017 Wolters Kluwer Health, Inc. All rights reserved.
Copyright © 2017 Wolters Kluwer Health, Inc. All rights reserved.

diagnostics. MDB thickness, rim volume, and BMO-MRW are 3 such parameters that demonstrate superiority to 2D RNFL circle scans, but show similar diagnostic capability when compared with each other. Future studies are required to expand upon our current knowledge of 3D parameters, their individual advantages, and how best to utilize them alongside other clinical markers for glaucoma.

REFERENCES

1. Tham YC, Li X, Wong TY, et al. Global prevalence of glaucoma and projections of glaucoma burden through 2040: a systematic review and meta-analysis. *Ophthalmology*. 2014;121: 2081–2090.
2. Chen TC. Spectral domain optical coherence tomography in glaucoma: qualitative and quantitative analysis of the optic nerve head and retinal nerve fiber layer (an AOS thesis). *Trans Am Ophthalmol Soc*. 2009;107:254–281.
3. Quigley HA, Addicks EM, Green WR. Optic nerve damage in human glaucoma. III. Quantitative correlation of nerve fiber loss and visual field defect in glaucoma, ischemic neuropathy, papilledema, and toxic neuropathy. *Arch Ophthalmol*. 1982; 100:135–146.
4. Sommer A, Katz J, Quigley HA, et al. Clinically detectable nerve fiber atrophy precedes the onset of glaucomatous field loss. *Arch Ophthalmol*. 1991;109:77–83.
5. Gabriele ML, Ishikawa H, Wollstein G, et al. Optical coherence tomography scan circle location and mean retinal nerve fiber layer measurement variability. *Invest Ophthalmol Vis Sci*. 2008;49:2315–2321.
6. Gurses-Ozden R, Ishikawa H, Hoh ST, et al. Increasing sampling density improves reproducibility of optical coherence tomography measurements. *J Glaucoma*. 1999;8:238–241.
7. Sehi M, Grewal DS, Sheets CW, et al. Diagnostic ability of fourier-domain vs time-domain optical coherence tomography for glaucoma detection. *Am J Ophthalmol*. 2009;148:597–605.
8. Van Der Schoot J, Vermeer KA, De Boer JF, et al. The effect of glaucoma on the optical attenuation coefficient of the retinal nerve fiber layer in spectral domain optical coherence tomography images. *Invest Ophthalmol Vis Sci*. 2012;53:2424–2430.
9. Wu H, De Boer JF, Chen TC. Reproducibility of retinal nerve fiber layer thickness measurements using spectral domain optical coherence tomography. *J Glaucoma*. 2011;20:470–476.
10. Kim NR, Lim H, Kim JH, et al. Factors associated with false positives in retinal nerve fiber layer color codes from spectral-domain optical coherence tomography. *Ophthalmology*. 2011; 118:1774–1781.
11. Moreno-Montanes J, Anton A, Olmo N, et al. Misalignments in the retinal nerve fiber layer evaluation using cirrus high-definition optical coherence tomography. *J Glaucoma*. 2011;20: 559–565.
12. Asrani S, Essaid L, Alder BD, et al. Artifacts in spectral-domain optical coherence tomography measurements in glaucoma. *JAMA Ophthalmol*. 2014;132:396–402.
13. Mitchell P, Hourihan F, Sandbach J, et al. The relationship between glaucoma and myopia: the Blue Mountains Eye Study. *Ophthalmology*. 1999;106:2010–2015.
14. Kim SY, Park HY, Park CK. The effects of peripapillary atrophy on the diagnostic ability of Stratus and Cirrus OCT in the analysis of optic nerve head parameters and disc size. *Invest Ophthalmol Vis Sci*. 2012;53:4475–4484.
15. Aref AA, Sayyad FE, Mwanza JC, et al. Diagnostic specificities of retinal nerve fiber layer, optic nerve head, and macular ganglion cell-inner plexiform layer measurements in myopic eyes. *J Glaucoma*. 2014;23:487–493.
16. Mwanza JC, Chang RT, Budenz DL, et al. Reproducibility of peripapillary retinal nerve fiber layer thickness and optic nerve head parameters measured with Cirrus HD-OCT in glaucomatous eyes. *Invest Ophthalmol Vis Sci*. 2010;51:5724–5730.
17. Arnalich-Montiel F, Munoz-Negrete FJ, Rebolleda G, et al. Cup-to-disc ratio: Agreement between slit-lamp indirect ophthalmoscopic estimation and Stratus optical coherence tomography measurement. *Eye*. 2007;21:1041–1049.
18. Leung CK, Choi N, Weinreb RN, et al. Retinal nerve fiber layer imaging with spectral-domain optical coherence tomography: Pattern of RNFL defects in glaucoma. *Ophthalmology*. 2010;117:2337–2344.
19. Chauhan BC, O'Leary N, Almobarak FA, et al. Enhanced detection of open-angle glaucoma with an anatomically accurate optical coherence tomography-derived neuroretinal rim parameter. *Ophthalmology*. 2013;120:535–543.
20. Gardiner SK, Ren R, Yang H, et al. A method to estimate the amount of neuroretinal rim tissue in glaucoma: Comparison with current methods for measuring rim area. *Am J Ophthalmol*. 2014;157:540–549. e541-542.
21. Schuman JS, Pedut-Kloizman T, Hertzmark E, et al. Reproducibility of nerve fiber layer thickness measurements using optical coherence tomography. *Ophthalmology*. 1996;103:1889–1898.
22. Simavli H, Que CJ, Akduman M, et al. Diagnostic capability of peripapillary retinal thickness in glaucoma using 3D volume scans. *Am J Ophthalmol*. 2015;159:545–556 e542.
23. Yang H, He L, Gardiner SK, et al. Age-related differences in longitudinal structural change by spectral-domain optical coherence tomography in early experimental glaucoma. *Invest Ophthalmol Vis Sci*. 2014;55:6409–6420.
24. Muth DR, Hirneiss CW. Structure-function relationship between Bruch's membrane opening-based optic nerve head parameters and visual field defects in glaucoma. *Invest Ophthalmol Vis Sci*. 2015;56:3320–3328.
25. Danthurebandara VM, Sharpe GP, Hutchison DM, et al. Enhanced structure-function relationship in glaucoma with an anatomically and geometrically accurate neuroretinal rim measurement. *Invest Ophthalmol Vis Sci*. 2015;56:98–105.
26. Chauhan BC, Danthurebandara VM, Sharpe GP, et al. Bruch's membrane opening minimum rim width and retinal nerve fiber layer thickness in a normal white population: a multicenter study. *Ophthalmology*. 2015;122:1786–1794.
27. Povazay B, Hofer B, Hermann B, et al. Minimum distance mapping using three-dimensional optical coherence tomography for glaucoma diagnosis. *J Biomed Opt*. 2007;12:041204.
28. Pollet-Villard F, Chiquet C, Romanet JP, et al. Structure-function relationships with spectral-domain optical coherence tomography retinal nerve fiber layer and optic nerve head measurements. *Invest Ophthalmol Vis Sci*. 2014;55:2953–2962.
29. Chen TC, Zeng A, Sun W, et al. Spectral domain optical coherence tomography and glaucoma. *Int Ophthalmol Clin*. 2008;48:29–45.
30. Lehmann OJ, Bunce C, Matheson MM, et al. Risk factors for development of post-trabeculectomy endophthalmitis. *Br J Ophthalmol*. 2000;84:1349–1353.
31. Staurenghi G, Sadda S, Chakravarthy U, et al. Proposed lexicon for anatomic landmarks in normal posterior segment spectral-domain optical coherence tomography: the international nomenclature for optical coherence tomography consensus. *Ophthalmology*. 2014;121:1572–1578.
32. Leung CK, Chan WM, Hui YL, et al. Analysis of retinal nerve fiber layer and optic nerve head in glaucoma with different reference plane offsets, using optical coherence tomography. *Invest Ophthalmol Vis Sci*. 2005;46:891–899.
33. Tsikata E, Lee R, Shieh E, et al. Comprehensive three-dimensional analysis of the neuroretinal rim in glaucoma using high-density spectral-domain optical coherence tomography volume scans. *Invest Ophthalmol Vis Sci*. 2016;57:5498–5508.
34. Shieh E, Lee R, Que C, et al. Diagnostic performance of a novel 3D neuroretinal rim parameter for glaucoma using high-density volume scans. *Am J Ophthalmol*. 2016;169:168–178.
35. Reis AS, Sharpe GP, Yang H, et al. Optic disc margin anatomy in patients with glaucoma and normal controls with spectral domain optical coherence tomography. *Ophthalmology*. 2012; 119:738–747.
36. Budenz DL, Michael A, Chang RT, et al. Sensitivity and specificity of the Stratus OCT for perimetric glaucoma. *Ophthalmology*. 2005;112:3–9.

Copyright © 2017 Wolters Kluwer Health, Inc. All rights reserved.

Copyright © 2017 Wolters Kluwer Health, Inc. All rights reserved.

37. Chen HY, Huang ML. Discrimination between normal and glaucomatous eyes using Stratus optical coherence tomography in Taiwan Chinese subjects. *Graefes Arch Clin Exp Ophthalmol*. 2005;243:894–902.
38. Schulze A, Lamparter J, Pfeiffer N, et al. Diagnostic ability of retinal ganglion cell complex, retinal nerve fiber layer, and optic nerve head measurements by fourier-domain optical coherence tomography. *Graefes Arch Clin Exp Ophthalmol*. 2011;249:1039–1045.
39. Nakatani Y, Higashide T, Ohkubo S, et al. Evaluation of macular thickness and peripapillary retinal nerve fiber layer thickness for detection of early glaucoma using spectral domain optical coherence tomography. *J Glaucoma*. 2011;20: 252–259.
40. Lu AT, Wang M, Varma R, et al. Combining nerve fiber layer parameters to optimize glaucoma diagnosis with optical coherence tomography. *Ophthalmology*. 2008;115:1352–1357. 1357 e1351-1352.
41. Sihota R, Sony P, Gupta V, et al. Diagnostic capability of optical coherence tomography in evaluating the degree of glaucomatous retinal nerve fiber damage. *Invest Ophthalmol Vis Sci*. 2006;47:2006–2010.
42. Leung CK, Mohamed S, Leung KS, et al. Retinal nerve fiber layer measurements in myopia: An optical coherence tomography study. *Invest Ophthalmol Vis Sci*. 2006;47:5171–5176.
43. Liu Y, Simavli H, Que CJ, et al. Patient characteristics associated with artifacts in spectralis optical coherence tomography imaging of the retinal nerve fiber layer in glaucoma. *Am J Ophthalmol*. 2015;159:565–576 e562.
44. Mwanza JC, Lee G, Budenz DL. Effect of adjusting retinal nerve fiber layer profile to fovea-disc angle axis on the thickness and glaucoma diagnostic performance. *Am J Ophthalmol*. 2016;161:12–21 e12.
45. Amini N, Nowroozizadeh S, Cirineo N, et al. Influence of the disc-fovea angle on limits of RNFL variability and glaucoma discrimination. *Invest Ophthalmol Vis Sci*. 2014;55:7332–7342.
46. He L, Ren R, Yang H, et al. Anatomic vs. Acquired image frame discordance in spectral domain optical coherence tomography minimum rim measurements. *PloS one*. 2014;9: e92225.

Copyright © 2017 Wolters Kluwer Health, Inc. All rights reserved.

Copyright © 2017 Wolters Kluwer Health, Inc. All rights reserved.